RESEARCH ARTICLE • OPEN ACCESS

Dynamic Simulations of Parkinson's Disease and ALS Propagation in the Brain: A Reaction-Diffusion on Brain Networks Approach

Zaidan Al Arsyad *et al.*

Volume 6, Issue 4, Pages 270–276, December 2025

Received 7 February 2025, Revised 18 March 2025, Accepted 9 September 2025, Published Online 20 November 2025

To Cite this Article : Z. A. Arsyad *et al.*,"Dynamic Simulations of Parkinson's Disease and ALS Propagation in the Brain: A Reaction-Diffusion on Brain Networks Approach", *Jambura J. Biomath*, vol. 6, no. 4, pp. 270–276, 2025, *https://doi.org/10.37905/jjbm.v6i4.30557*

JOURNAL INFO • JAMBURA JOURNAL OF BIOMATHEMATICS

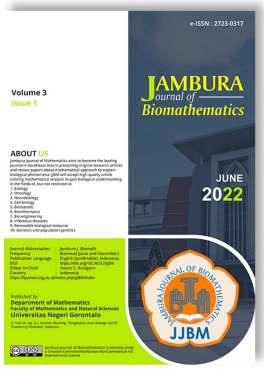

Homepage	:	http://ejurnal.ung.ac.id/index.php/JJBM/index
Journal Abbreviation	:	Jambura J. Biomath.
Frequency	:	Quarterly (March, June, September and December)
Publication Language	:	English
DOI	:	https://doi.org/10.37905/jjbm
Online ISSN	:	2723-0317
Editor-in-Chief	:	Hasan S. Panigoro
Publisher	:	Department of Mathematics, Universitas Negeri Gorontalo
Country	:	Indonesia
OAI Address	:	http://ejurnal.ung.ac.id/index.php/jjbm/oai
Google Scholar ID	:	XzYgeKQAAAAJ
Email	:	editorial.jjbm@ung.ac.id

JAMBURA JOURNAL • FIND OUR OTHER JOURNALS

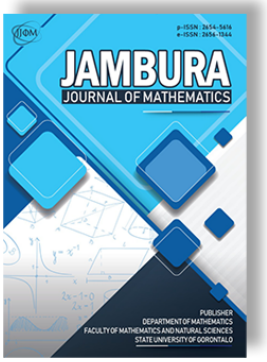

Jambura Journal of Mathematics

Jambura Journal of Mathematics Education

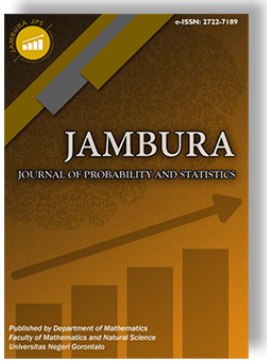

Jambura Journal of Probability and Statistics

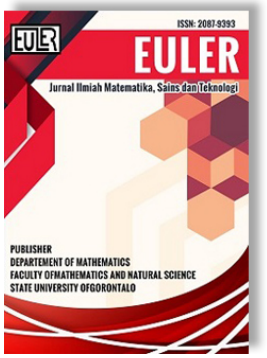

EULER : Jurnal Ilmiah Matematika, Sains, dan Teknologi

Jambura Journal of Biomathematics, Volume 6, Issue 4, Pages 270–276, December 2025 https://doi.org/10.37905/jjbm.v6i4.30557

Research Article

Check for updates

Dynamic Simulations of Parkinson's Disease and ALS Propagation in the Brain: A Reaction-Diffusion on Brain Networks Approach

Zaidan Al Arsyad[1], Faiz Munir[1], Amanda Allawiyah[1], Tiara Sania[1], Irvan Hartawan[1], and Prama Putra[2,3,*]

[1]*Undergraduate Mathematics Study Program, Institut Teknologi Bandung, Indonesia*
[2]*Faculty of Mathematics and Natural Sciences, Institut Teknologi Bandung, Indonesia*
[3]*Center for Mathematical Modelling and Simulation, Institut Teknologi Bandung, Indonesia*

ARTICLE HISTORY
Received 7 February 2025
Revised 18 March 2025
Accepted 9 September 2025
Published 20 November 2025

KEYWORDS
Reaction-diffusion
Graph laplacian
Brain connectome
Parkinson's
Amyotropic lateral sclerosis

ABSTRACT. *Neurodegenerative diseases, such as Parkinson's Disease (PD) and Amyotrophic Lateral Sclerosis (ALS), progressively degrade neural systems, leading to considerable cognitive functional disorders. It is consequential to comprehend how these diseases spread within the brain to develop precise diagnoses and interventions. This study uses a reaction-diffusion model on a human brain network model to explore and replicate the actual dynamic progression of PD and ALS. By incorporating diffusion processes with empirical brain network data, we simulated the disease's progression through various regions. Our results show unique propagation patterns for PD and ALS and the effect of different network models on disease transmission. The structure of brain neural networks plays a vital function in neurodegeneration and offers insights that lead to early detection and focused treatments. This study presents a potential viewpoint on handling and interfering in neurodegenerative diseases by perceiving their dependency on brain neural connectivity.*

1. Introduction

Neurodegenerative diseases are a group of disorders that are primarily affecting the nervous system. Many diseases result in progressive loss of cognitive function and, ultimately, a diagnosis of dementia. For instance, the decline of mental functions, loss of short-term memory, and decreased bodily functions in the late stage of the disease are common characteristics of these diseases [1, 2]. Parkinson's disease (PD) and amyotrophic lateral sclerosis (ALS), for example, pose substantial health challenges due to their incapacitating effects and increasing prevalence in the elderly [3]. It is believed that such interference is associated with neuronal death, brain atrophy, and overall cognitive decline because of pathological protein aggregates throughout the brain. Although there have been significant strides in comprehending these illnesses, the exact processes driving their progression in the brain are still not fully understood.

The progression of PD and ALS involves intricate interactions among genetic, molecular, and environmental factors, leading to the gradual loss of neurons and severe motor dysfunction [4]. Currently, the progression of these diseases can be traced through the distribution of pathological protein aggregates in the brain [2, 5–7]. However, studies on unraveling the systematic propagation on neurodegenerative diseases focuses more on Alzheimer's disease, while PD and ALS are quite limited. Quantitative studies of PD and ALS lack on understanding the whole-brain propagation. Our study investigates this gap, especially on PD and ALS, and highlights the important roles of initial seeding location in the brain associated with the disease progression. By providing deeper insight into the dynamics of these diseases, this approach identifies key pathways and vulnerable network nodes that could be targeted with new treatments [8].

In our effort to understand PD and ALS, we employ an innovative method by simulating protein propagation in the brain connectome using a reaction-diffusion model on brain networks. While this approach has yielded significant insights [9], it is important to recognize its limitations: (1) Observation Limitation – The study focuses on the spread of protein deposits, the primary cause of PD and ALS, but does not explore the fundamental causes of initial damage and protein accumulation; (2) Cause and Effect – The study does not examine how protein accumulation and brain damage affect cognitive and motor abilities, leaving a gap in understanding the impact of these diseases on daily life and functionality; (3) Prevention and Cure – The study does not investigate the prevention or treatment of these diseases, limiting its scope by not offering insights into potential therapeutic approaches. The central question guiding this study is: How do the propagation patterns of Parkinson's disease and Amyotrophic Lateral Sclerosis (ALS) occur within the brain?

This study aims to replicate the propagation patterns of PD and ALS within the brain using mathematical modelling. By

*Corresponding Author.

Email : *prama.putra@itb.ac.id* (P. Putra)
Homepage : http://ejurnal.ung.ac.id/index.php/JJBM/index / E-ISSN : 2723-0317

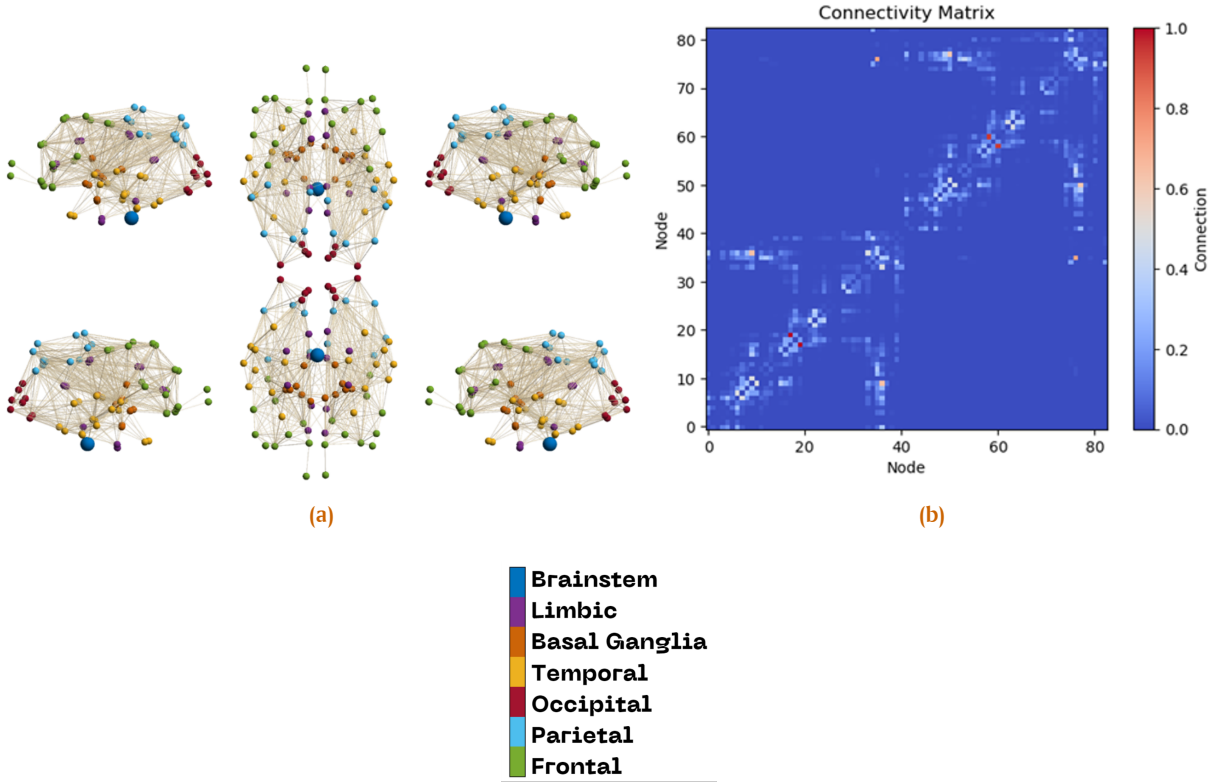

Figure 1. (a) Six representative subgraphs of point of view from the full 83-node network, showing regional connectivity (e.g., frontal, limbic, parietal). Colors indicate anatomical lobes. (b) Adjacency matrix for the full network, where entries A_{ij} encode connection weights between nodes i and j. The matrix corresponds to the network in (a).

employing a reaction-diffusion model on brain networks, it seeks to simulate how these neurodegenerative diseases spread across different brain regions. The goal is to understand the underlying dynamics of disease progression, providing a detailed framework that reflects the complex interactions within neural circuits. This modelling approach will help identify critical factors influencing disease spread and could pave the way for developing targeted therapeutic interventions.

Although reaction-diffusion models have been commonly used to study Alzheimer's disease [6, 7], their application to PD and ALS—particularly in quantifying the role of brain network topology in prion-like propagation—remains limited. Our work addresses this gap by integrating empirical connectome data with a reaction-diffusion framework to uncover disease-specific spreading patterns, offering a new perspective on PD and ALS progression.

We start our study by constructing a mathematical reaction-diffusion model on brain networks. We then explain the computation for determining the order of disease progression patterns using a rank model. Our method is tested on three different brain network weighting schemes. Our simulations indicate that different network weighting schemes influence propagation patterns. Specifically, capturing the ALS progression pattern requires seeding from two initial brain locations, unlike PD, which typically involves one brain region.

Our seeding hypotheses align with established pathological staging. For PD, The Braak staging system [10] posits that α-synuclein pathology originates in the brain stem (single node) before spreading to limbic and cortical regions. For ALS, TDP-43 pathology often arises independently in motor cortex and spinal cord (multiple nodes), as observed in cross-sectional studies [11, 12].

2. Model Formulation

To gain a comprehensive understanding of neurodegeneration in the human brain, mathematical and computational modelling are crucial and advantageous. Our model incorporates the prion-like paradigm and intracellular transport mechanisms [13–16]. A physics-based approach enhances the mathematical model by including reaction terms that describe the proliferation of misfolded proteins [17–23]. This nonlinear interaction, combined with a diffusive process, offers a more detailed view of prion-like propagation within the brain. The mathematical model we consider is presented by

$$\frac{\mathrm{d}c_i}{\mathrm{d}t} = -\rho \sum_{j=1}^{N} A_{ij}(c_j - c_i) + \alpha c_i(1 - c_i), \tag{1}$$

where $c_i = c_i(t)$ denotes a toxic protein concentration at node i. The concentration evolves on a network $G = (V, E)$ of size N which is represented by an adjacency matrix $\mathbf{A} = [A_{ij}]$ with size $N \times N$. The edges E of network G represent connections between nodes V on that network. The first summation term represents the graph Laplacian, quantifying the diffusion flux between node i and its neighbours. It represents the diffusion of the toxic protein across the brain network, capturing protein

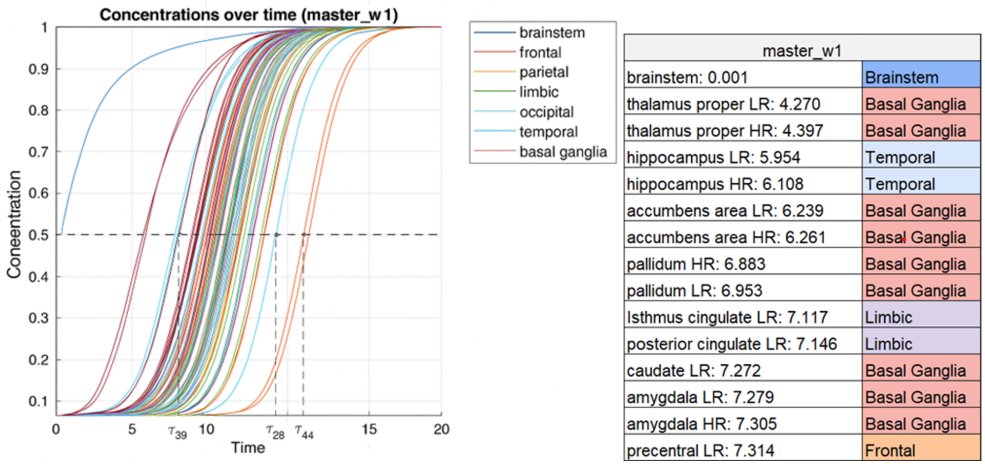

master_w1	
brainstem: 0.001	Brainstem
thalamus proper LR: 4.270	Basal Ganglia
thalamus proper HR: 4.397	Basal Ganglia
hippocampus LR: 5.954	Temporal
hippocampus HR: 6.108	Temporal
accumbens area LR: 6.239	Basal Ganglia
accumbens area HR: 6.261	Basal Ganglia
pallidum HR: 6.883	Basal Ganglia
pallidum LR: 6.953	Basal Ganglia
Isthmus cingulate LR: 7.117	Limbic
posterior cingulate LR: 7.146	Limbic
caudate LR: 7.272	Basal Ganglia
amygdala LR: 7.279	Basal Ganglia
amygdala HR: 7.305	Basal Ganglia
precentral LR: 7.314	Frontal

Figure 2. (a) Evolution of $C_i(t)$ for selected nodes (e.g., node 39, 28, 44) with threshold $T = 0.5$. Dashed line marks arrival time τ_j when $C_j(\tau_j) = T$. (b) Ranked arrival times. The earliest nodes to reach T are listed with the name of the node and region in order, demonstrating the simulated staging pattern. This subset corresponds to the initial propagation wave observed in (a).

transport between connected brain regions according to the adjacency matrix **A**. The second term models local protein growth via a logistic function, reflecting intra-node aggregation and saturation dynamics. Parameters α and ρ represent the growth and diffusion rates, respectively. This model has been discussed in a paper in which the growth of the toxic protein is given by a logistic process and the propagation is given by a diffusive process, represented by the graph Laplacian. Due to undefined parameter values of the model, we rescale the model with $t \approx 1/\alpha$ and we have

$$\frac{\mathrm{d}c_i}{\mathrm{d}t} = -\kappa \sum_{j=1}^{N} A_{ij}(c_j - c_i) + c_i(1 - c_i), \tag{2}$$

where $\kappa = \rho_\alpha$ denotes the ratio between the diffusion and growth rates. This rescaling simplifies parameter exploration and focuses the model on the interplay between protein spread and proliferation. The initial condition is $c_s(0) > 0$ for seeding nodes s, otherwise $c_i(0) = 0$.

The growth rate (α) and diffusion coefficient (ρ) were selected based on empirical data: $\alpha \in [0.01, 0.1]$ matches the doubling time of α-synuclein in PD[24] and TDP-43 in ALS[11], while $\rho \in [0.001, 0.1]$ reflects measured protein spreading rates[7, 14]. The ratio $\kappa = \rho/\alpha$ (0.01–10) spans were chosen by combining extreme values of α and ρ. Minimum κ (0.01) occurs when the weakest ρ (0.001) divided by the fastest α (0.1). Maximum κ (10) occurs when ρ is the fastest (0.1) and α is the weakest (0.01).

We use the brain connectome to represent brain network connectivity in our simulation. The connectome is a discrete model of the human brain, consisting of nodes and edges that represent parcellated brain regions and their interactions [25–27]. In this study, we focus on structural connectomes, which are often utilized to study brain function and the progression of neurodegenerative diseases. We employ individual patient data in GraphML format obtained from BrainGraph.org [25, 26]. These structural connectomes are constructed using the Lausanne multi-resolution atlas parcellation. For our study, we limit the scope to an 83-node brain graph.

We tested three weighting schemes: (1) length-free (uniform connectivity), (2) ballistic transport (mimicking active axonal transport at constant velocity [16, 25], and (3) diffusive transport (simulating passive protein spreading [13, 27]). These schemes reflect distinct biophysical mechanisms of protein propagation in neurodegeneration. The connections between nodes in the brain are represented by an idealized uniform cylinder composed of n_{ij} fibres with length l_{ij}. Figure 1 illustrates the brain connectome and its sample weighted adjacency matrix.

3. Numerical Results

3.1. Arrival Time and Staging Computation

We assume that the system's dynamics begin with an initial condition where all concentrations are zero except in a few nodes. The system then evolves asymptotically until all concentrations reach their maximum value. Let Ω_j for $j = 1, \ldots, J$ be a collection of non-overlapping nodes such that $\Omega_j \subseteq V$ and $\Omega_j \cap \Omega_k = \emptyset$ if $j \neq k$. Let $T \in [0, 1]$ be an arbitrary threshold value. As the concentration evolves according to eq. (2), we define the average concentration C_j at node j,

$$C_j = \frac{1}{|\Omega_j|} \sum_{i \in \Omega_j}^{J} c_j, \qquad j = 1, \ldots, J, \tag{3}$$

and record the time when C_j first reaches the threshold T such that $C_j(\tau_j) = T$. These times τ_j are referred to as the arrival times. This process generates an ordering of the regions Ω_j based on their arrival times. The ordered sequence $\{\Omega_1, \Omega_2, \ldots, \Omega_J\}$ is known as an observed staging pattern. The generalized staging problem involves determining the range of observable staging patterns by varying κ in eq. (2). Ultimately, we can compare the observed staging patterns to one or more desirable staging patterns derived from empirical studies [15].

Figure 2 illustrates the computation of the arrival times of different nodes $(\tau_{39}, \tau_{28}, \tau_{44})$ with threshold 0.5 as the initial value given is 0.5 at the seeding node. From the concentration trajectories in Figure 2a, we extract the arrival times τ_j when nodes first exceed the threshold $T = 0.5$. Figure 2b shows the

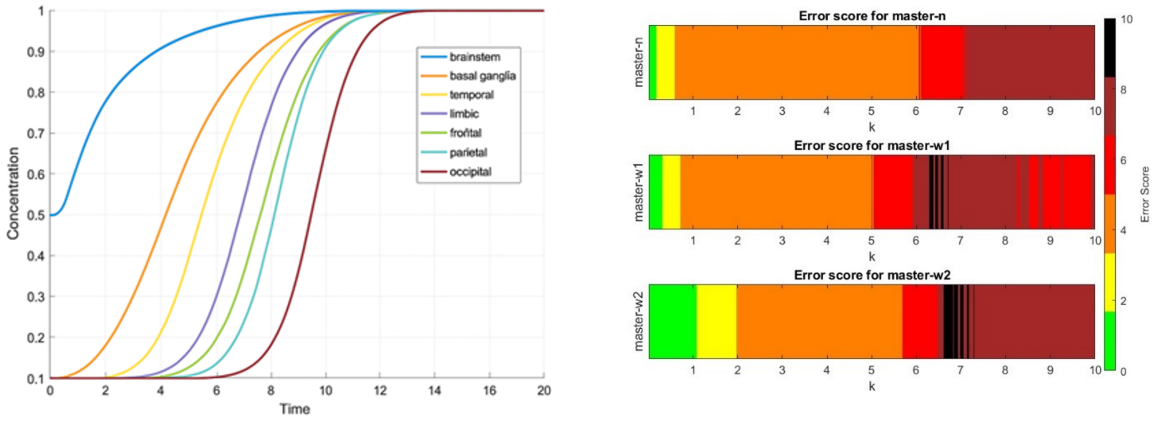

(a) (b)

Figure 3. (a) Evolution of protein concentration over time for PD simulation using parameter $\kappa = 0.2$ with the master-w2 adjacency matrix. Each curve corresponds to the fastest node in distinct brain regions (brainstem, basal ganglia, temporal, limbic, frontal, parietal, and occipital). (b) Error score heatmaps comparing three network weighting schemes (master-n, master-w1, master-w2) over a range of κ values. Green color indicates minimal error (exact match with literature staging), while red and darker color indicates higher deviation.

ranked arrival sequence of the fastest-propagating nodes in a table, which determines the simulated staging order. The list continues until 83 nodes are written. Figure 2b are cut to show the first fastest 15 nodes. This ranking is later compared to empirical data (Figure 3b and Figure 4b) to compute error scores.

3.2. *Error Score for Rank Comparison*

Error score (e) describes the magnitude of the error in the order of simulation results compared to the literature. This score provides a quantitative measure of how closely the simulated results align with the established rankings found in the literature. By using a ranking system, the simulation results are compared against the reference rankings from the literature. If the order of the simulation results deviates significantly from the literature order, the error score will increase accordingly. This means that a larger error score indicates a greater discrepancy between the simulation and the literature rankings, highlighting the extent to which the simulation results differ from the expected or known outcomes.

The error score is calculated by determining the sum of the absolute differences between the ranks of the simulation results and the ranks from the literature. This method ensures that each deviation, regardless of its direction, contributes positively to the overall error score. Consequently, a higher total of these absolute differences signifies a larger error score, reflecting a greater misalignment between the simulated and the reference rankings.

4. Discussion

To observe the propagation of Parkinson's and ALS diseases, we need the values of the parameter κ as explained earlier. Based on literature studies, the growth coefficient of the proteins that cause Parkinson's and ALS diseases ranges from 0.01 to 0.1, while the diffusion coefficient ranges from 0.001 to 0.1. Consequently, a range of values for k is obtained, spanning from 0.01 to 10. Subsequently, discretization is performed with $\Delta = 0.01$ to observe the simulation of the spread of Parkinson's and ALS diseases for the aforementioned range of κ. Thus, the simulation is conducted 1000 times.

The concentration growth graphs in Figure 3a illustrate the progression of Parkinson's Disease over time for the fastest nodes representing each brain region. All simulations for Parkinson's Disease maintain a consistent initial condition where node 83 (brain stem) starts with a concentration value of 0.5, while all other nodes begin at 0. The specific example shown here uses the master-w2 adjacency matrix with $\kappa = 0.2$. On the x-axis, time is represented, and on the y-axis, concentration. Each line in the graph corresponds to a different brain region, demonstrating how concentration changes over time. The legend indicates the various brain regions and the exact nodes representing each brain region in this example are the brain stem (node 83), basal ganglia (node 76), temporal (node 81), limbic (node 56), frontal (node 51), parietal (node 57), and occipital (node 65).

This figure is an example from thousands of simulations conducted. We determine the staging in our simulation by identifying which node in each brain region reaches a concentration of 0.5 first. Observations from this figure indicate that the brain stem reaches the 0.5 concentration threshold first, followed sequentially by the basal ganglia, temporal, limbic, frontal, parietal, and occipital regions. This order reflects the typical progression of Parkinson's Disease, starting from the brain stem and spreading to other regions at varying rates.

To ascertain the order in which brain regions reach the 0.5 concentration threshold, we analysed the concentration growth across all 83 nodes post-iteration. Each brain region was ranked based on the earliest node to reach a 0.5 concentration. This analysis was repeated 3000 times, accounting for three different adjacency matrices and 1000 different values of κ. Figure 3a exemplifies the outcome of one such simulation.

After obtaining the orders for all matrix and κ variations, we compared these results with the literature to identify the

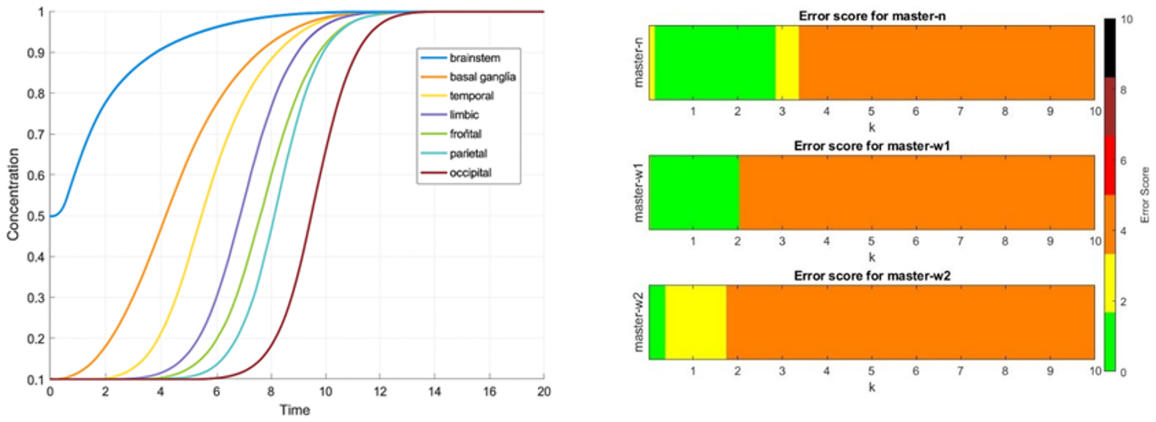

(a) (b)

Figure 4. (a) Protein concentration evolution over time for ALS simulation with parameter $\kappa = 0.2$ using the master-w1 adjacency matrix. Curves represent the fastest nodes in brainstem, basal ganglia, temporal, limbic, frontal, parietal, and occipital regions. Initial seeding includes frontal (nodes 10, 51) and brainstem (node 83) with different concentrations. (b) Error score heatmaps for ALS simulations showing the fit of different network weighting schemes across κ values. The green area indicates best agreement with literature staging patterns for ALS progression.

variations that best match documented progression patterns of Parkinson's Disease. Comparing the simulation stages with the literature is essential for validation, aligning our simulation outputs with the known spread of α-synuclein in the brain. The error score visualizations in Figure 3b illustrate this comparison. The x-axis represents the value of κ, while the color spectrum represents the error score. The color gradient indicates the level of deviation from the literature, with green representing an error score of 0 (indicating an exact match with the literature) and red indicating higher deviations. The three subplots correspond to the adjacency matrices: master-n (top), master-w1 (middle), and master-w2 (bottom).

The error score analysis in Figure 3b demonstrates that the master-w2 adjacency matrix with k values between 0.01 and 1.10 shows the least deviation from the literature, indicating the highest accuracy in simulating Parkinson's Disease progression. This finding highlights the suitability of the master-w2 matrix with these k values for accurately modelling the disease's spread.

The concentration growth graphs in Figure 4a illustrate the progression of ALS over time for the fastest nodes representing each brain region. Unlike the Parkinson's Disease simulations, ALS simulations have different initial conditions. For ALS, nodes 10 and 51 (frontal) start with concentration values of 0.5, while node 83 (brain stem) starts with a concentration of 0.1. All other nodes begin with a concentration of 0. This setup reflects literature findings that ALS typically first manifests in the frontal region and then progresses to the brain stem. Unlike Parkinson's simulations, which only initialize the first stage in the brain stem, ALS simulations include initial values for both the frontal and brain stem stages to ensure that the simulation ranks align with literature observations. If we only initiated the frontal region, the simulation results would not match the literature.

In this example, we use the master-w1 adjacency matrix with $\kappa = 0.2$. The x-axis represents time, and the y-axis represents concentration. Each line in the graph corresponds to a different brain region, showing how concentration changes over time. The legend indicates the various brain regions and the exact nodes representing each brain region in this example are the brain stem (node 83), basal ganglia (node 78), temporal (node 75), limbic (node 55), frontal (node 10), parietal (node 11), and occipital (node 63). This figure is an example from thousands of simulations conducted. To determine the staging in our simulation, we identify which node in each brain region first reaches a concentration of 0.5. Observations from this figure illustrate the sequence in which different brain regions reach the 0.5 concentration threshold, providing insights into the progression of ALS in the brain.

To determine the order in which brain regions reach the 0.5 concentration threshold, we analyzed the concentration growth across all 83 nodes after the iterations. Each brain region was ranked based on the earliest node to reach a 0.5 concentration. This process was repeated 3000 times, using three different adjacency matrices and 1000 different values of κ. Figure 4(a) exemplifies the result of one such simulation.

Due to the limited literature on ALS progression, our comparison only considers the progression across four brain regions: frontal, brain stem, parietal, and basal ganglia. The literature often mentions stages occurring in smaller regions within these larger brain regions and stages involving the spinal cord, which our model does not represent. As our method uses representative nodes, we do not account for these repetitions and lack a spinal cord node. Consequently, we focused on the primary regions mentioned. The error score visualizations in Figure 4b illustrate this comparison. The x-axis represents the value of κ, and the color spectrum represents the error score. The color gradient indicates the level of deviation from the literature, with green representing an error score of 0 (indicating that the simulation order matches the literature exactly) and red representing higher deviations. The three subplots correspond to the adjacency matrices: master-n (top), master-w1 (middle), and master-

Table 1

Disease	Optimal Network Weighting	Approximate κ Range Showing Best Fit	Minimum Error Score	Initial Seeding Nodes
Parkinson's	master-w2	0.01 - 1.10	0	Node 83 (Brain stem)
Amyotrophic Lateral Sclerosis	master-n	0.15 - 2.80	0	Nodes 10 & 51 (Frontal), 83 (Brain stem)

w2 (bottom).

The error score analysis in Figure 4b demonstrates that the master-n adjacency matrix with k values between 0.15 and 2.80 shows the least deviation from the literature, indicating the highest accuracy in simulating ALS progression. This finding highlights the suitability of the master-n matrix with these k values for accurately modelling the disease's spread. While our model supports multi-focal seeding in ALS, we acknowledge that the exact number of seeding sites may vary across individuals. Future work should incorporate patient-specific pathology data to refine these assumptions [27].

The results summarized in Table 1 highlight the distinct propagation characteristics of PD and ALS as captured by our modeling approach. For Parkinson's Disease, the master-w2 weighting scheme combined with a parameter range of $\kappa = 0.01 - 1.10$ yields the closest fit to known disease progression patterns, with a single seeding node in the brain stem (node 83). ALS progression is best modeled using the master-n weighting scheme with values of $\kappa = 0.15 - 2.80$, requiring multiple seeding nodes primarily in the frontal region (nodes 10 and 51) in addition to the brain stem (node 83). The minimum error scores of zero in both cases confirm that these configurations provide accurate reproduction of empirical staging sequences.

5. Conclusion

In conclusion, this study has shown that our mathematical reaction-diffusion model is robust and effective for accurately replicating the spread of both ALS and Parkinson's disease. The model's success in capturing the dynamics of these neurodegenerative diseases suggests it could be a valuable tool for understanding how these diseases progress. For Parkinson's disease, we found that the master-w2 provided the most reliable simulation results. This is because it closely matches the observed data, which has the widest range of k compared to master-n and master-w1 and has the least deviation from the literature, which validates the model's accuracy. In contrast, for ALS, the master-n emerged as the most effective which has the widest range of k compared to master-w1 and master-w2 and has the least deviation from the literature, showing a strong correlation with actual disease spread patterns and proving to be highly suitable for modelling ALS progression. These findings not only deepen our understanding of how ALS and Parkinson's spread but also pave the way for future research to refine and optimize mathematical models for other neurodegenerative diseases. Our results could help develop targeted therapeutic strategies and improve predictive capabilities in clinical settings.

For future research, we suggest doing the simulation with different values of α and ρ, so that the equation will no longer be dimensionless and hopefully the accuracy of the simulation will be increased. We can also reduce some of the assumptions to better reflect actual cases and consider adding other variables, like medications that can slow the progression of the disease.

Author Contributions. **Arsyad, Z. A.**: Mathematical simulation, writing the manuscript: original draft preparation and review and editing. **Munir, F.**: Mathematical simulation, writing the manuscript: original draft preparation. **Allawiyah, A.**: Mathematical simulation and visualization. **Sania, T.**: Mathematical simulation and visualization. **Hrtawan, I.**: Mathematical simulation and visualization. **Putra, P.**: Conceptualization of the study, methodology, supervision, writing the manuscript: review and editing.

Acknowledgement. We gratefully acknowledge the funding from the ITB research grant under Program PPMI FMIPA 2024 no. 92/IT1.C02/SK-TA/2024 for PP. We made use of AI for paraphrasing and improvising our written English for our manuscript.

Funding. The funding of this research was from the ITB research grant under Program PPMI FMIPA 2024 no. 92/IT1.C02/SK-TA/2024 for PP.

Conflict of interest. The authors declare no competing interests and no conflicts of interest to report regarding the present study.

Data availability. Not applicable.

References

[1] C. R. Jack *et al.*, "Prevalence of biologically vs clinically defined alzheimer spectrum entities using the national institute on aging–alzheimer's association research framework," *JAMA neurology*, vol. 76, no. 10, pp. 1174–1183, 2019. DOI:10.1001/jamaneurol.2019.1971

[2] C. R. Jack *et al.*, "Tracking pathophysiological processes in alzheimer's disease: an updated hypothetical model of dynamic biomarkers," *The lancet neurology*, vol. 12, no. 2, pp. 207–216, 2013. DOI:10.1016/S1474-4422(12)70291-0

[3] J. Sun *et al.*, "Hospital-treated infections in early-and mid-life and risk of alzheimer's disease, parkinson's disease, and amyotrophic lateral sclerosis: a nationwide nested case-control study in sweden," *PLoS Medicine*, vol. 19, no. 9, p. e1004092, 2022. DOI:10.1371/journal.pmed.1004092

[4] S. Y. Pang *et al.*, "The interplay of aging, genetics and environmental factors in the pathogenesis of parkinson's disease," *Translational Neurodegeneration*, vol. 8, no. 1, p. 23, 2019. DOI:10.1186/s40035-019-0165-9

[5] K. A. Johnson *et al.*, "Brain imaging in alzheimer disease," *Cold Spring Harbor perspectives in medicine*, vol. 2, no. 4, p. a006213, 2012. DOI:10.1101/cshperspect.a006213

[6] M. Jucker and L. C. Walker, "Propagation and spread of pathogenic protein assemblies in neurodegenerative diseases," *Nature neuroscience*, vol. 21, no. 10, pp. 1341–1349, 2018. DOI:10.1038/s41593-018-0238-6

[7] M. Jucker and L. C. Walker, "Self-propagation of pathogenic protein aggregates in neurodegenerative diseases," *Nature*, vol. 501, no. 7465, pp. 45–51, 2013. DOI:10.1038/nature12481

[8] A. Liu *et al.*, "Unraveling the intercellular communication disruption and key pathways in alzheimer's disease: an integrative study of single-nucleus transcriptomes and genetic association," *Alzheimer's Research & Therapy*, vol. 16, no. 1, p. 3, 2024. DOI:10.1186/s13195-023-01372-w

[9] O. Schmitt *et al.*, "Reaction-diffusion models in weighted and directed connectomes," *PLoS Computational Biology*, vol. 18, no. 10, p. e1010507, 2022. DOI:10.1371/journal.pcbi.1010507

[10] H. Braak *et al.*, "Staging of brain pathology related to sporadic parkinson's disease," *Neurobiology of aging*, vol. 24, no. 2, pp. 197–211, 2003. DOI:10.1016/s0197-4580(02)00065-9

[11] C. Tian *et al.*, "Erythrocytic α-synuclein as a potential biomarker for parkinson's disease," *Translational neurodegeneration*, vol. 8, no. 1, p. 15, 2019. DOI:10.1186/s40035-019-0155-y

[12] J. Brettschneider *et al.*, "Stages of ptdp-43 pathology in amyotrophic lateral sclerosis," *Annals of neurology*, vol. 74, no. 1, pp. 20–38, 2013. DOI:10.1002/ana.23937

[13] J. Weickenmeier *et al.*, "A physics-based model explains the prion-like features of neurodegeneration in alzheimer's disease, parkinson's disease, and amyotrophic lateral sclerosis," *Journal of the Mechanics and Physics of Solids*, vol. 124, pp. 264–281, 2019. DOI:10.1016/j.jmps.2018.10.013

[14] J. Weickenmeier, E. Kuhl, and A. Goriely, "Multiphysics of prionlike diseases: Progression and atrophy," *Physical review letters*, vol. 121, no. 15, p. 158101, 2018. DOI:10.1103/PhysRevLett.121.158101

[15] P. Putra *et al.*, "Front propagation and arrival times in networks with application to neurodegenerative diseases," *SIAM Journal on Applied Mathematics*, vol. 83, no. 1, pp. 194–224, 2023. DOI:10.1137/21M1467547

[16] P. Putra *et al.*, "Braiding braak and braak: Staging patterns and model selection in network neurodegeneration," *Network Neuroscience*, vol. 5, no. 4, pp. 929–956, 2021. DOI:10.1162/netn_a_00208

[17] G. S. Brennan and A. Goriely, "A network aggregation model for amyloid-β dynamics and treatment of alzheimer's diseases at the brain scale," *Journal of Mathematical Biology*, vol. 90, no. 2, p. 22, 2025. DOI:10.1007/s00285-024-02179-5

[18] G. S. Brennan *et al.*, "The role of clearance in neurodegenerative diseases," *SIAM Journal on Applied Mathematics*, vol. 84, no. 3, pp. S172–S198, 2023. DOI:10.1137/22M1487801

[19] M. Goedert, M. Masuda-Suzukake, and B. Falcon, "Like prions: the propagation of aggregated tau and α-synuclein in neurodegeneration," *Brain*, vol. 140, no. 2, pp. 266–278, 2017. DOI:10.1093/brain/aww230

[20] A. Raj *et al.*, "Combined model of aggregation and network diffusion recapitulates alzheimer's regional tau-positron emission tomography," *Brain connectivity*, vol. 11, no. 8, pp. 624–638, 2021. DOI:10.1089/brain.2020.0841

[21] A. Raj *et al.*, "Network diffusion model of progression predicts longitudinal patterns of atrophy and metabolism in alzheimer's disease," *Cell reports*, vol. 10, no. 3, pp. 359–369, 2015. DOI:10.1016/j.celrep.2014.12.034

[22] A. Raj, A. Kuceyeski, and M. Weiner, "A network diffusion model of disease progression in dementia," *Neuron*, vol. 73, no. 6, pp. 1204–1215, 2012. DOI:10.1016/j.neuron.2011.12.040

[23] T. B. Thompson *et al.*, "Protein-protein interactions in neurodegenerative diseases: A conspiracy theory," *PLoS computational biology*, vol. 16, no. 10, p. e1008267, 2020. DOI:10.1371/journal.pcbi.1008267

[24] L. M. Smith *et al.*, "α-synuclein and anti-α-synuclein antibodies in parkinson's disease, atypical parkinson syndromes, rem sleep behavior disorder, and healthy controls," *PLoS One*, vol. 7, no. 12, p. e52285, 2012. DOI:10.1371/journal.pone.0052285

[25] B. Szalkai *et al.*, "Parameterizable consensus connectomes from the human connectome project: the budapest reference connectome server v3. 0," *Cognitive neurodynamics*, vol. 11, no. 1, pp. 113–116, 2017. DOI:10.1007/s11571-016-9407-z

[26] B. Szalkai *et al.*, "The budapest reference connectome server v2. 0," *Neuroscience Letters*, vol. 595, pp. 60–62, 2015. DOI:10.1016/j.neulet.2015.03.071

[27] M. Xia, J. Wang, and Y. He, "Brainnet viewer: a network visualization tool for human brain connectomics," *PloS one*, vol. 8, no. 7, p. e68910, 2013. DOI:10.1371/journal.pone.0068910